nature neuroscience

Control of glioblastoma tumorigenesis by feed-forward cytokine signaling

Arezu Jahani-Asl[1–5], Hang Yin[3,6–8], Vahab D Soleimani[5,9], Takrima Haque[4,5], H Artee Luchman[10], Natasha C Chang[3,6], Marie-Claude Sincennes[3,6], Sidharth V Puram[1], Andrew M Scott[11], Ian A J Lorimer[3,12], Theodore J Perkins[3,6,12], Keith L Ligon[13,14], Samuel Weiss[10], Michael A Rudnicki[3,6] & Azad Bonni[1,2]

EGFRvIII-STAT3 signaling is important in glioblastoma pathogenesis. Here, we identified the cytokine receptor OSMR as a direct target gene of the transcription factor STAT3 in mouse astrocytes and human brain tumor stem cells (BTSCs). We found that OSMR functioned as an essential co-receptor for EGFRvIII. OSMR formed a physical complex with EGFRvIII, and depletion of OSMR impaired EGFRvIII-STAT3 signaling. Conversely, pharmacological inhibition of EGFRvIII phosphorylation inhibited the EGFRvIII-OSMR interaction and activation of STAT3. EGFRvIII-OSMR signaling in tumors operated constitutively, whereas EGFR-OSMR signaling in nontumor cells was synergistically activated by the ligands EGF and OSM. Finally, knockdown of *OSMR* strongly suppressed cell proliferation and tumor growth of mouse glioblastoma cells and human BTSC xenografts in mice, and prolonged the lifespan of these mice. Our findings identify OSMR as a critical regulator of glioblastoma tumor growth that orchestrates a feed-forward signaling mechanism with EGFRvIII and STAT3 to drive tumorigenesis.

Glioblastoma is the most common malignant primary brain tumor in adults. Despite advances in understanding the molecular mechanisms underlying these tumors, current treatments are ineffective[1–5]. Therefore, there is an urgent need to better understand the pathogenesis of these devastating tumors.

Glioblastoma tumors are thought to arise from astrocytes and their precursors, neural stem cells[6–10]. Regardless of the cell of origin, the resulting tumors are a heterogeneous population composed of both undifferentiated and differentiated cells and contain a subpopulation of tumorigenic self-renewing BTSCs[11–14]. The identification of BTSCs within glioblastoma tumors has raised intense interest in the identification of mechanisms that regulate the tumorigenic property of these cells.

Among frequent genetic alterations identified in glioblastoma tumors are activating mutations of epidermal growth factor receptor (EGFR), which transform both immortalized mouse astrocytes and neural stem cells into malignant tumor cells[4,7,15–17]. The most common active mutant of EGFR in glioblastoma is a truncated EGFR in which exons 2–7 are deleted (EGFRvIII)[16]. EGFRvIII is a constitutively active receptor that in the absence of epidermal growth factor (EGF) induces the phosphorylation of STAT3 to drive tumorigenesis[17,18]. However, the mechanisms by which STAT3 drives glial cell transformation and the malignant behavior of human BTSCs in the background of EGFR activation remain poorly understood. In this study, we identified the cytokine receptor OSMR as a critical component of EGFRvIII-STAT3 signaling that triggers a feed-forward signaling mechanism to drive the pathogenesis of glioblastoma.

RESULTS

EGFRvIII-STAT3 transcriptional targets in glioblastoma

To facilitate identification of differentially expressed genes induced by EGFRvIII-STAT3 signaling in human BTSCs, we performed RNA sequencing (RNA-seq) analysis of three EGFRvIII-expressing BTSC lines: BTSC68, BTSC73 and BTSC90 (**Supplementary Tables 1**,**2**, and **Supplementary Fig. 1a–c**). As a control, we performed RNA-seq on a BTSC line that does not express EGFRvIII, BTSC41. Differentially expressed genes in each of BTSC68, BTSC73 and BTSC90 lines were called relative to the BTSC41 control by Tophat/Cufflinks RNA-seq analysis pipeline. Intersection of differentially regulated genes in each of the EGFRvIII-expressing BTSCs was obtained, and 272 common candidate targets were identified in human BTSCs (**Fig. 1a**, **Supplementary Fig. 1c**,**d** and **Supplementary Tables 3** and **4**).

To identify candidate target genes of EGFRvIII-STAT3 signaling in astrocytes specifically in an EGFRvIII- or STAT3-dependent manner, we used a genetic mouse model. We analyzed EGFRvIII-expressing or control MSCV-infected astrocytes that expressed *Stat3* (*Stat3*$^{loxP/loxP}$)

[1]Department of Neurobiology, Harvard Medical School, Boston, Massachusetts, USA. [2]Department of Neuroscience, Washington University School of Medicine, St. Louis, Missouri, USA. [3]Ottawa Hospital Research Institute, Ottawa, Ontario, Canada. [4]Department of Oncology, McGill University, Montreal, Quebec, Canada. [5]Lady Davis Institute for Medical Research, Jewish General Hospital, Montreal, Quebec, Canada. [6]Department of Cellular and Molecular Medicine, University of Ottawa, Ottawa, Ontario, Canada. [7]Department of Biochemistry, University of Georgia, Athens, Georgia, USA. [8]Molecular Biology Centre for Molecular Medicine, University of Georgia, Athens, Georgia, USA. [9]Department of Human Genetics, McGill University, Montreal, Quebec, Canada. [10]Department of Cell Biology & Anatomy, University of Calgary, Calgary, Alberta, Canada. [11]Olivia Newton-John Cancer Research Institute, School of Cancer Medicine, La Trobe University, Melbourne, Australia. [12]Department of Biochemistry, Microbiology and Immunology, University of Ottawa, Ottawa, Ontario, Canada. [13]Dana-Farber Cancer Institute, Harvard Medical School, Boston, Massachusetts, USA. [14]Department of Pathology, Harvard Medical School, Boston, Massachusetts, USA. Correspondence should be addressed to A.J.-A. (arezu.jahani@mcgill.ca), M.A.R. (mrudnicki@ohri.ca) or A.B. (bonni@wustl.edu).

Received 29 January; accepted 31 March; published online 25 April 2016; doi:10.1038/nn.4295

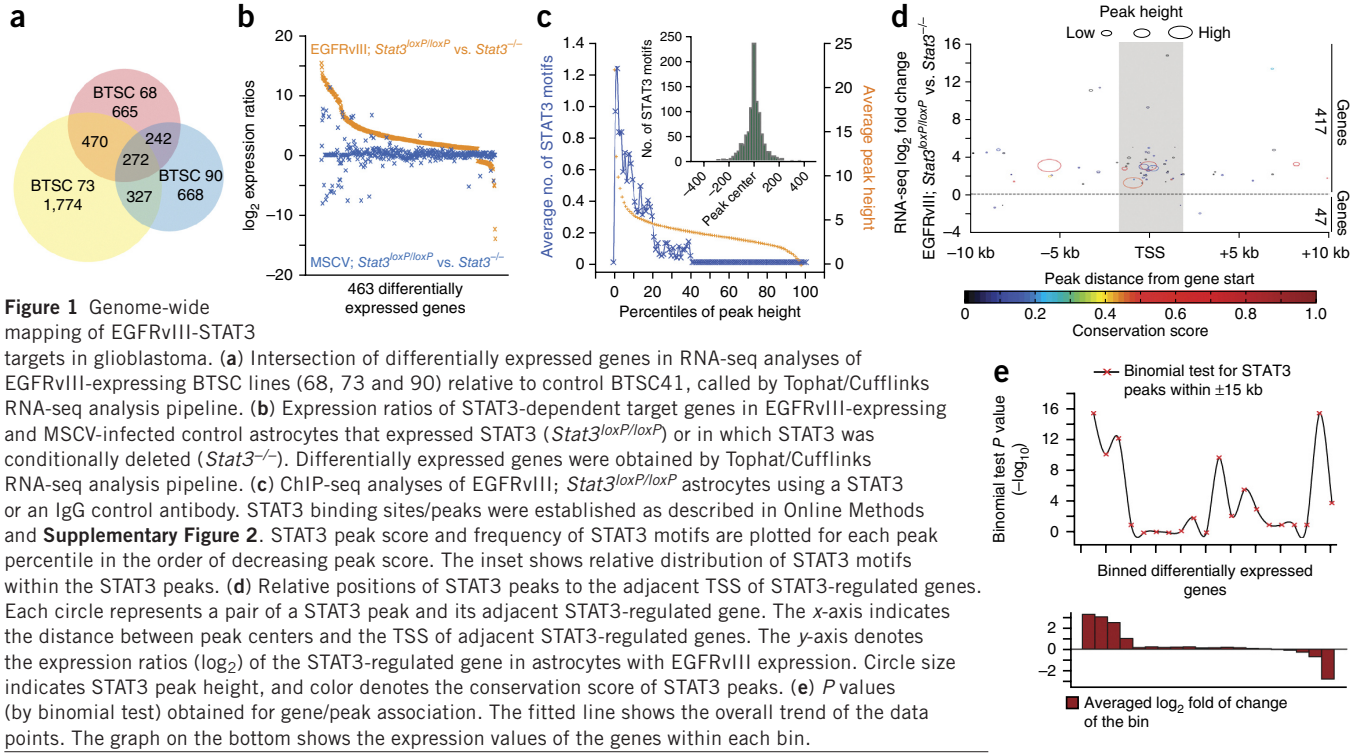

Figure 1 Genome-wide mapping of EGFRvIII-STAT3 targets in glioblastoma. (**a**) Intersection of differentially expressed genes in RNA-seq analyses of EGFRvIII-expressing BTSC lines (68, 73 and 90) relative to control BTSC41, called by Tophat/Cufflinks RNA-seq analysis pipeline. (**b**) Expression ratios of STAT3-dependent target genes in EGFRvIII-expressing and MSCV-infected control astrocytes that expressed STAT3 (*Stat3*$^{loxP/loxP}$) or in which STAT3 was conditionally deleted (*Stat3*$^{-/-}$). Differentially expressed genes were obtained by Tophat/Cufflinks RNA-seq analysis pipeline. (**c**) ChIP-seq analyses of EGFRvIII; *Stat3*$^{loxP/loxP}$ astrocytes using a STAT3 or an IgG control antibody. STAT3 binding sites/peaks were established as described in Online Methods and **Supplementary Figure 2**. STAT3 peak score and frequency of STAT3 motifs are plotted for each peak percentile in the order of decreasing peak score. The inset shows relative distribution of STAT3 motifs within the STAT3 peaks. (**d**) Relative positions of STAT3 peaks to the adjacent TSS of STAT3-regulated genes. Each circle represents a pair of a STAT3 peak and its adjacent STAT3-regulated gene. The *x*-axis indicates the distance between peak centers and the TSS of adjacent STAT3-regulated genes. The *y*-axis denotes the expression ratios (log_2) of the STAT3-regulated gene in astrocytes with EGFRvIII expression. Circle size indicates STAT3 peak height, and color denotes the conservation score of STAT3 peaks. (**e**) *P* values (by binomial test) obtained for gene/peak association. The fitted line shows the overall trend of the data points. The graph on the bottom shows the expression values of the genes within each bin.

or in which *Stat3* was conditionally deleted (*Stat3*$^{-/-}$) by RNA-seq (**Supplementary Fig. 1e**). We established differentially regulated genes in an EGFRvIII- and STAT3-dependent manner. Most genes that were highly induced in a STAT3-dependent manner in EGFRvIII-expressing astrocytes displayed little or no induction in response to STAT3 in the absence of EGFRvIII expression (**Fig. 1b**).

In parallel, we used chromatin immunoprecipitation followed by massively parallel sequencing (ChIP-seq) to identify genome-wide sites of STAT3 occupancy in the background of EGFRvIII expression. We defined high-confidence STAT3 binding sites (STAT3 peaks) based on STAT3 motif and conservation scores (**Fig. 1c** and **Supplementary Fig. 2a–d**). In analyzing the genomic distribution of STAT3 ChIP-seq peaks relative to the STAT3 differentially regulated genes, we found that STAT3 operates primarily as a transcriptional activator in EGFRvIII-expressing astrocytes (**Fig. 1d,e**) and that STAT3 peaks were most abundant in the 5′ untranslated region (UTR) and promoter relative to genes (**Fig. 1d** and **Supplementary Fig. 2e,f**).

To identify EGFRvIII-STAT3 direct target genes that might have a role in the pathogenesis of glioblastoma, we focused on target genes with the following features: (i) STAT3 occupancy of the promoter or 5′ UTR, (ii) upregulated expression in a STAT3-dependent manner, (iii) conservation of STAT3 ChIP-seq peaks and STAT3 binding motifs across 20 placental mammals within ± 5 kilobases (kb) of the transcription start site (TSS), and (iv) differential expression in the same direction in all EGFRvIII-expressing human BTSCs and mouse astrocytes.

OSMR, EGFRvIII and STAT3 share a common gene network

RNA-seq analyses revealed that *OSMR* was highly expressed in all EGFRvIII-expressing human BTSCs and mouse astrocytes (**Supplementary Fig. 1c,e**). ChIP-seq analyses revealed that STAT3 robustly occupied the promoter of the *OSMR* gene (**Supplementary Fig. 3e**). In analyses of gene expression of human glioblastoma tumor samples deposited in The Cancer Genome Atlas (TCGA) and REMBRANDT databases, upregulation of both *STAT3* and *OSMR* in human glioblastoma patients correlated significantly with worse patient prognosis (**Fig. 2a,b** and **Supplementary Fig. 3a,b**), suggesting that *OSMR* may be a critical STAT3 target gene in the pathogenesis of human glioblastoma. In performing multivariate analyses using two independent approaches of Cox proportional hazards and stratified logrank test, we found that there was significant association of *OSMR* and *STAT3* upregulation with reduced survival in glioma patients even when taking into consideration *IDH1* mutation status, patient age and tumor grade ($P < 0.01$, **Supplementary Fig. 3c,d**). These analyses suggest that the expression levels of *OSMR* and *STAT3* are important predictors of survival.

We confirmed by ChIP followed by quantitative PCR (ChIP-qPCR) that STAT3 directly occupied the promoter of the *OSMR* gene in human BTSCs expressing EGFRvIII or exhibiting high levels of phosphorylated STAT3 (**Fig. 2c,d**, **Supplementary Table 1**). Likewise, STAT3 directly occupied the promoter of the *Osmr* gene in EGFRvIII-expressing mouse astrocytes (**Supplementary Fig. 3f**). Deletion of *Stat3* resulted in profound reduction in the levels of OSMR protein and *Osmr* mRNA in EGFRvIII-expressing astrocytes (**Supplementary Fig. 3g,h**). Knockdown of *Stat3* in BTSC73 cells using a lentiviral-mediated RNA interference approach triggered the downregulation of *Osmr* mRNA levels (**Supplementary Fig. 3i**). Immunoblotting analyses showed that OSMR protein expression was also higher in EGFRvIII-expressing human BTSCs and mouse astrocytes, compared to BTSCs and astrocytes that did not express EGFRvIII (**Supplementary Figs. 1a** and **3g**). Taken together, these data support the conclusion that OSMR is a direct EGFRvIII-STAT3 target gene.

We next characterized the landscape of OSMR target genes in the background of EGFRvIII expression. We performed RNA-seq analyses on two different *OSMR* knockdown (OSMR-KD1 and OSMR-KD2) and two control (scramble small hairpin (sh)RNA control and vector control) EGFRvIII-expressing astrocyte lines. We established

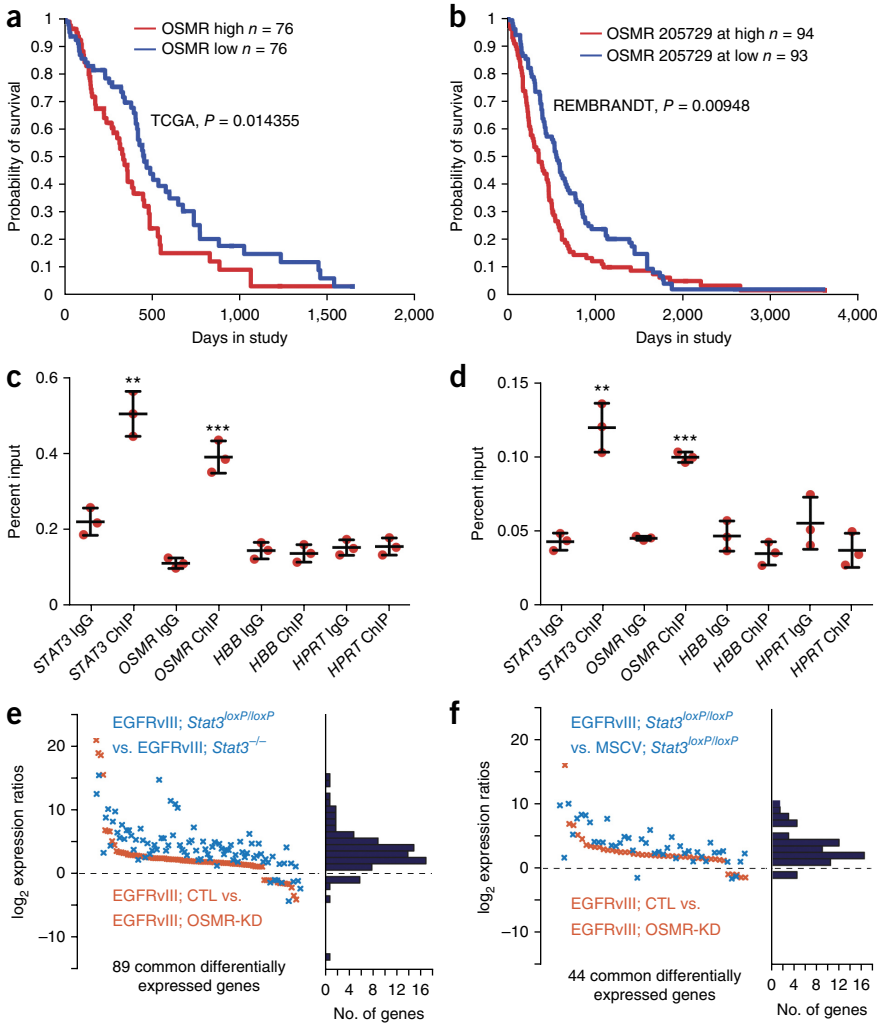

Figure 2 *OSMR* is a direct transcriptional target gene of STAT3 that shares a common network of genes with EGFRvIII and STAT3. (**a**,**b**) OSMR Kaplan-Meier survival plots for glioblastoma patients with elevated OSMR levels using TCGA (**a**) and REMBRANDT (**b**) databases as described in Online Methods. Significance of difference between the two groups was computed by the chi-squared statistic. (**c**) Immunoprecipitation of lysates from BTSC73 using a STAT3 antibody or IgG control followed by analyses by RT-q-PCR. STAT3 was used as positive control. *HPRT* and *HBB* were used as negative controls. Data are representative of three independent replicates. *STAT3*: $P = 0.002$, $t = 7.114$, d.f. = 4; *OSMR*: $P = 0.0004$, $t = 10.87$, d.f. = 4; *HBB*: $P = 0.72$, $t = 0.385$, d.f. = 4; *HPRT*: $P = 0.89$, $t = 0.15$, d.f. = 4. Error bars represent ± s.e.m. (**d**) ChIP-PCR of lysates from BTSC145 analyzed as in **c**. Data are representative of three independent replicates. *STAT3*: $P = 0.002$, $t = 7.63$, d.f. = 4; *OSMR*: $P = 0.0001$, $t = 24.9$, d.f. = 4; *HBB*: $P = 0.19$, $t = 1.57$, d.f. = 4; *HPRT*: $P = 0.20$, $t = 1.51$, d.f. = 4. Error bars represent ± s.e.m. $^{**}P < 0.01$; $^{***}P < 0.001$. (**e**,**f**) Differentially expressed genes that were up- or downregulated in an OSMR-dependent manner, established by RNA-seq and intersected with STAT3- or EGFRvIII-regulated genes. STAT3, OSMR and EGFRvIII regulate the expression of a common gene network (Fisher's exact test) $P = 2.2 \times 10^{-16}$). CTL, control; *Osmr*-KD, *Osmr* knockdown.

OSMR-regulated genes and compared them with STAT3- and EGFRvIII-dependent candidate target genes. We found significant overlap between OSMR-dependent and STAT3-dependent or EGFRvIII-dependent targets (89 and 44 genes, respectively; **Fig. 2e**,**f**). These results suggest that OSMR is a positive feed-forward signal with the EGFRvIII-STAT3 pathway in glioblastoma pathogenesis.

EGFRvIII and OSMR are co-receptors

Our finding that OSMR has a common network of target genes with EGFRvIII led us to the hypothesis that OSMR and EGFRvIII form a co-receptor complex. Immunohistochemical analyses using OSMR and EGFRvIII antibodies revealed that these two proteins co-localized at the membrane (**Supplementary Fig. 4a**,**b**). OSMR is thought to associate with gp130 to form a high-affinity receptor for its ligands[19]. Therefore, we immunoprecipitated lysates of EGFRvIII-expressing BTSCs or astrocytes using an OSMR antibody followed by immunoblotting with EGFR, EGFRvIII and gp130 antibodies. We found that OSMR interacted with EGFRvIII endogenously in both mouse astrocytes and human BTSCs (**Fig. 3a**,**b**). However, we did not detect the interaction of endogenous OSMR with gp130 or wild-type EGFR in EGFRvIII-expressing human BTSCs and mouse astrocytes (**Fig. 3a**,**b** and **Supplementary Fig. 4c**). To confirm the EGFRvIII-OSMR interaction *in situ*, we used a proximity ligation assay (PLA) with antibodies recognizing OSMR or activated EGFR that is phosphorylated on Tyr1068. We found that endogenous OSMR interacted with phosphorylated EGFR-Y1068 and EGFRvIII in EGFRvIII-expressing human BTSCs (**Fig. 3c**) compared to the non-EGFRvIII-expressing control human BTSC12 and BTSC139 lines (**Fig. 3d**).

EGFRvIII may induce secretion of cytokines resulting in gp130 activation in a paracrine fashion to maintain tumor growth and heterogeneity in mixed composition glioblastoma tumors[20]. Because we did not detect direct interaction of gp130 or wild-type EGFR with OSMR in EGFRvIII-expressing cells, we asked whether gp130 or wild-type EGFR might indirectly mediate the interaction of EGFRvIII and OSMR. Using PLAs, we assessed binding of OSMR and EGFRvIII in *gp130* knockdown or wild-type *EGFR* knockdown, EGFRvIII-expressing astrocytes. Immunoblotting analyses confirmed efficient knockdown of wild-type EGFR and gp130 (**Supplementary Fig. 4d**,**e**). Knockdown of gp130 or EGFR had little or no effect on the EGFRvIII-OSMR interaction (**Supplementary Fig. 4f**). Further, STAT3 activation was not reduced in EGFRvIII-expressing astrocytes upon knockdown of genes encoding gp130 or wild-type EGFR (**Supplementary Fig. 4g**). These data suggest that gp130 and wild-type EGFR are not required for the interaction of EGFRvIII with OSMR.

Next, we characterized the role of oncostatin M (OSM), the ligand for OSMR, in signal transduction by the EGFRvIII-OSMR co-receptor complex. We analyzed tumorigenic GFP-EGFRvIII-expressing and non-tumorigenic GFP-MSCV-expressing control astrocytes treated with OSM or EGF by PLA to examine the association of EGFR or EGFRvIII with OSMR. In EGFRvIII-expressing astrocytes, we detected the association with OSMR in the absence of OSM or EGF treatment (**Fig. 3e**,**i**). In the absence of ligand treatment, PLA did

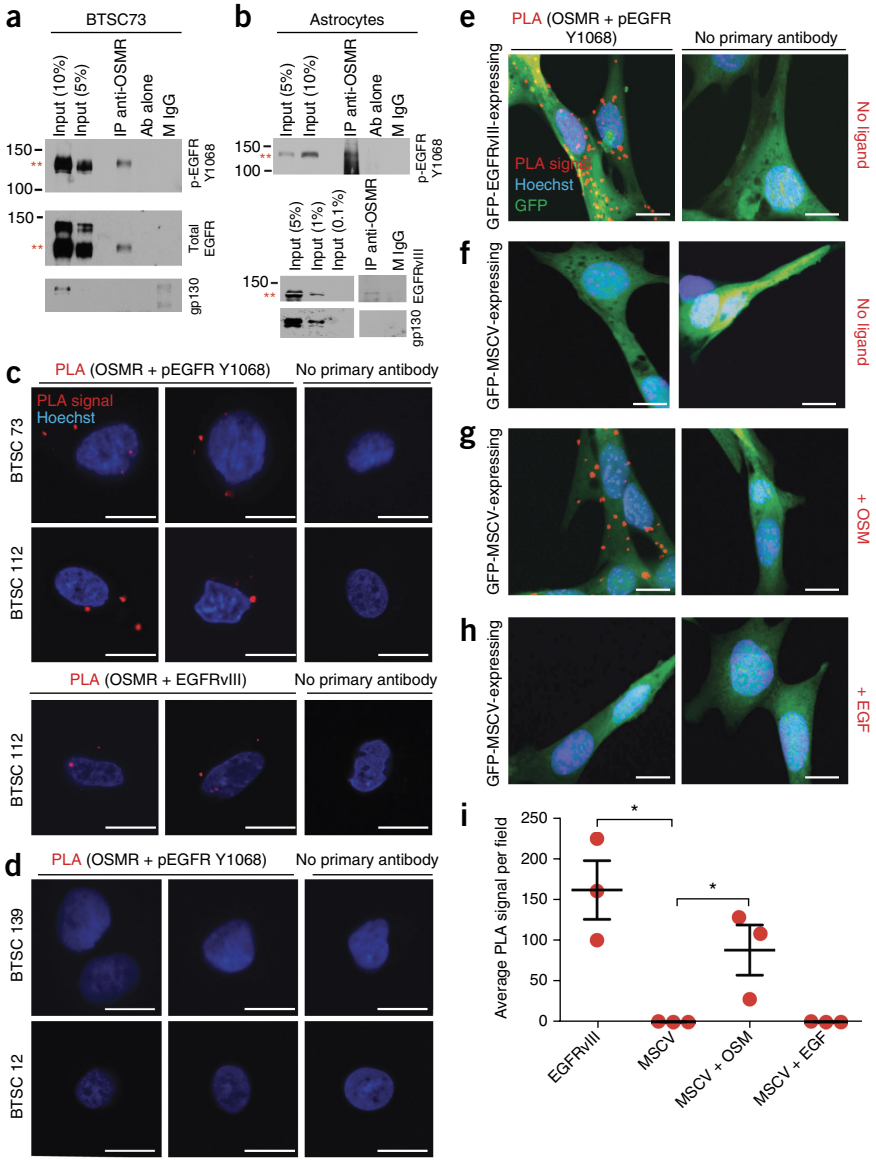

Figure 3 OSMR interacts with EGFRvIII in EGFRvIII-expressing mouse astrocytes and human BTSCs. (**a**,**b**) Immunoprecipiation (IP) of lysates of EGFRvIII-expressing BTSC73 (**a**) and EGFRvIII-expressing mouse astrocytes (**b**) with an OSMR antibody (IP anti-OSMR) or a mouse IgG (M IgG) control followed by immunoblotting with indicated antibodies (Ab). Full-length blots are presented in **Supplementary Figure 7**. EGFRvIII is marked with **. (**c**,**d**) PLA of OSMR and activated EGFR in BTSCs performed using OSMR antibodies and either of pEGFR-Tyr1068 or EGFRvIII antibodies in EGFRvIII-expressing BTSC lines (73 and 112) (**c**) or in BTSC lines that did not express EGFRvIII (12 and 139) (**d**). Primary antibodies were omitted for the control. Red dots represent interaction signal. Nuclei were stained with the DNA dye bisbenzimide (Hoechst). Representative images from analyses of two independent slides are shown. Scale bars, 10 μm. (**e**–**h**) PLA of OSMR and activated EGFR performed using the OSMR and pEGFR-Y1068 antibodies in tumorigenic GFP-EGFRvIII-expressing astrocytes and non-tumorigenic GFP-MSCV-expressing astrocytes in the absence or presence of EGF and OSM. Representative images from analyses of three independent slides are shown. Scale bars, 10 μm. (**i**) PLA signal in **e**–**h** quantified across three random fields from three independent slides. Significance of difference was analyzed by unpaired *t*-test, two tail distribution, EGFRvIII versus MSCV: $P = 0.011$, $t = 4.497$, d.f. = 4; MSCV versus MSCV + OSM: $P = 0.04$, $t = 3.037$, d.f. = 4; MSCV versus MSCV + EGF: $P = 0.99$, $t = 0.0$, d.f. = 4. *$P < 0.05$. Error bars represent ± s.e.m.

not reveal interaction between OSMR and EGFR in MSCV-infected control astrocytes (**Fig. 3f**,**i**). By contrast, OSM treatment stimulated robust interaction of OSMR with EGFR in the control astrocytes (**Fig. 3g**,**i**). Notably, EGF treatment was not sufficient to stimulate the EGFR-OSMR interaction in astrocytes (**Fig. 3h**,**i**). Because OSM is required to trigger the interaction of OSMR with EGFR in astrocytes that do not express oncogenic EGFRvIII, we assessed the influence of OSM on EGFR and STAT3 signaling in these cells. Treatment of MSCV-control astrocytes with OSM robustly induced the activation of EGFR as reflected by its phosphorylation at Y1068, and led to the activation of STAT3 as detected by phosphorylation of STAT3 at Tyr705 and Ser727 (**Fig. 4a** and **Supplementary Fig. 5a–e**). The functional consequence of OSM addition to non-tumorigenic MSCV-expressing astrocytes was a significant increase in the proliferative capacity of these cells as quantified by Ki67 staining (unpaired Student's *t* test, two-tailed distribution, $P = 0.01$, $n = 3$, **Supplementary Fig. 5f–h**). The addition of OSM and EGF induced the synergistic phosphorylation of STAT3 at Ser727 in wild-type astrocytes (**Fig. 4b**,**c** and **Supplementary Fig. 5e**). These results support the conclusion that activated/phosphorylated EGFR and OSMR function in a complex to regulate cell growth and that OSM signaling induces the phosphorylation of EGFR, leading to the EGFR-OSMR interaction.

We next addressed the question of whether phosphorylation of EGFR or of EGFRvIII is required for the OSMR-EGFRvIII interaction. We determined the effect of two pharmacological inhibitors of EGFR-EGFRvIII phosphorylation, canertinib and lapatinib, on the EGFRvIII-OSMR interaction in astrocytes. We first confirmed that both inhibitors substantially attenuated the phosphorylation of EGFRvIII (**Fig. 4d**). The addition of either inhibitor impaired the binding of EGFRvIII to OSMR (**Fig. 4e**, lapatinib treatment) and the phosphorylation of STAT3 (**Fig. 4d**). These results suggest that the phosphorylation of EGFRvIII may regulate its binding with OSMR and that the EGFRvIII-OSMR interaction in the absence of ligand occurs owing to the constitutive phosphorylation of EGFRvIII. Conversely, exposure of wild-type astrocytes to exogenous OSM is required to trigger an increase in the phosphorylation of EGFR and consequently its interaction with OSMR, and STAT3 signaling. Knockdown of *OSMR* substantially reduced the levels of EGFRvIII (**Fig. 4f**), suggesting that OSMR may also control the stability of EGFRvIII in addition to its phosphorylation status. Accordingly, knockdown of *OSMR* also substantially reduced the phosphorylation of STAT3 at the key regulatory sites Tyr705 and Ser727 (**Fig. 4f**) suggesting that OSMR is required to maintain STAT3 signaling in EGFRvIII-expressing astrocytes. Taken together, our data indicate that EGFRvIII and OSMR are obligate co-receptors.

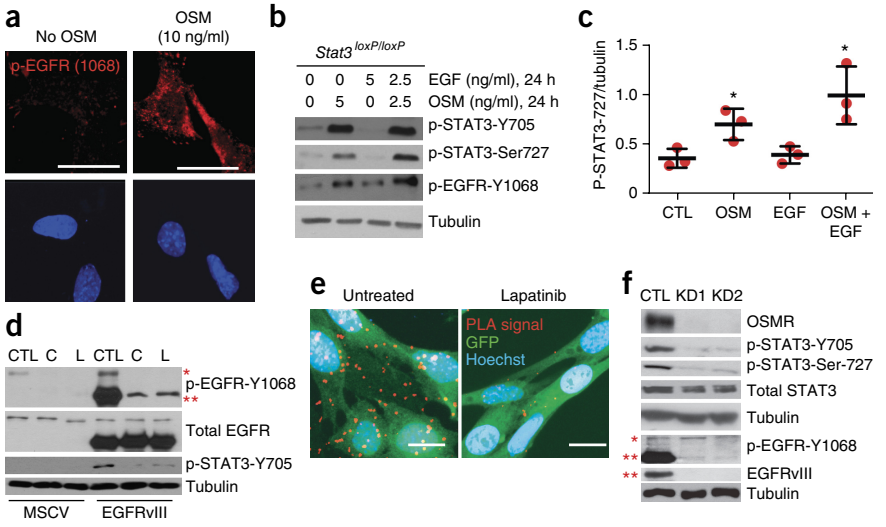

Figure 4 The ligand OSM regulates the phosphorylation of EGFR and the pharmacological inhibitors of EGFRvIII phosphorylation impair EGFRvIII-OSMR interaction. (**a**) Immunohistochemical analyses of wild-type astrocytes, treated with 10 ng/ml of OSM, and assessed by using the pEGFR-Y1068 antibody. Image is representative of six random fields from two independent slides. Scale bars, 20 μm. (**b**) Treatment of non-tumorigenic astrocytes with combined EGF and OSM and analyses of STAT3 phosphorylation using the p-STAT3-Ser727 antibody. Full-length blots are presented in **Supplementary Figure 7**. (**c**) Quantification of p-STAT3-Ser727 levels in **b** by performing densitometric analyses using ImageJ ($n = 3$, unpaired t-test, two tail distribution, OSM treated versus control: $P = 0.032$, $t = 3.2$, d.f. = 4; OSM + EGF versus control: $P = 0.023$, $t = 3.58$, d.f. = 4; EGF versus control: $P = 0.67$, $t = 0.45$, d.f. = 4. $^*P < 0.05$. Error bars represent ± s.e.m. (**d**) Immunoblot of tumorigenic GFP-EGFRvIII-expressing astrocytes and non-tumorigenic GFP-MSCV-expressing astrocytes treated with either lapatinib or carnitinib, and analyzed using indicated antibodies. Blot is representative of two independent biological replicates. Full-length blots are presented in **Supplementary Figure 7**. (**e**) GFP-EGFRvIII-expressing astrocytes that were treated with lapatinib were subjected to PLA of OSMR and EGFRvIII as described in **Figure 3**. Images are representative of six random fields across two independent slides. Scale bars, 10 μm. (**f**) EGFRvIII-expressing mouse *Osmr*-KD1, -KD2, and vector control (CTL) astrocytes were analyzed by immunoblotting. P-STAT3-Y705 and P-STAT3-Ser727 antibodies were used to assess STAT3 phosphorylation. The p-EGFR-Y1068 antibody was used to examine EGFRvIII and EGFR phosphorylation levels. EGFRvIII antibody is used to detect total EGFRvIII levels. Tubulin was used as loading control. Full-length blots are presented in **Supplementary Figure 7**. The blots represent a minimum of three technical replicates from different passage number for each cell line. In all blots, total EGFR and EGFRvIII are indicated with * and **, respectively.

OSMR stimulates the proliferation of BTSCs and astrocytes

Since EGFRvIII-STAT3 signaling has a key role in the regulation of cell growth, we examined the role of OSMR in the regulation of cell growth. We generated three different OSMR knockdown BTSC73 lines by lentivirus-mediated delivery of three independent shRNAs targeting *OSMR* mRNA. We confirmed that each of the three shRNAs induced the efficient knockdown of endogenous *OSMR*, reducing *OSMR* mRNA levels by 65–77% in BTSC73 cells (**Supplementary Fig. 6a**,**b**). We found that the knockdown of *OSMR* significantly reduced the population growth of EGFRvIII-expressing BTSC73 cells (**Fig. 5a**,**b**).

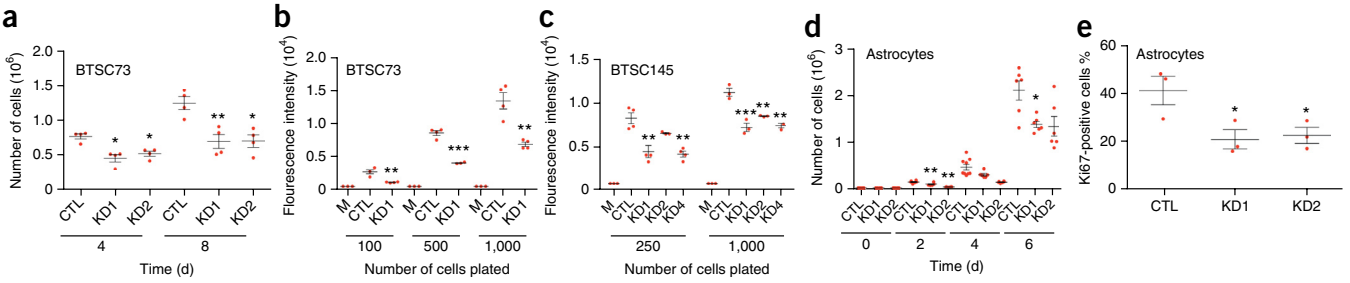

Figure 5 OSMR regulates cell growth of EGFRvIII-expressing astrocytes and brain tumor stem cells. (**a**) EGFRvIII-expressing BTSC73-OSMR-knockdown lines and corresponding scramble control were cultured in 6 well plates for 4 d and 8 d, after which cells in each well were counted. Graph represents cell counts at different time points for each group. Significance of difference was analyzed by unpaired t-test, two tail distribution, $n = 3$ for 4-day studies, $n = 4$ for 8-day studies. CTL vs. KD1, 4 d: $P = 0.0227$, $t = 3.6$, d.f. = 4; CTL vs. KD2, 4 d: $P = 0.0287$, $t = 3.345$, d.f. = 4; CTL vs. KD1, 8 d: $P = 0.0071$, $t = 4.003$, d.f. = 6; CTL vs. KD2, 8 d; $P = 0.006$, $t = 4.153$, d.f. = 6. $^*P \le 0.05$; $^{**}P \le 0.01$; $^{***}P \le 0.001$). Error bars represent ± s.e.m. (**b**) 100, 500, and 1000 cells were plated for each of *OSMR*-KD1- and scrambled control-BTSC73 lines. Cell viability was confirmed using Alamar blue following 1 week in culture. Medium alone (M) was used to measure background signal. Fluorescence intensity for each BTSC line is plotted ($n = 4$ technical replicates for each cell line, unpaired t-test, two tail distribution. CTL vs. KD1, 100 cells: $P = 0.0015$, $t = 5.479$, d.f. = 6; CTL vs. KD1, 500 cells: $P = 0.0001$, $t = 12.54$, d.f. = 6; CTL vs. KD1, 1,000 cells: $P = 0.002$, $t = 5.158$, d.f. = 6. Error bars represent ± s.e.m. (**c**) Cell growth was assessed in BTSC145-knockdown lines (*hOSMR*-KD1, -KD2, and -KD3) and corresponding scramble control and data analyses was performed as described in b. $n = 3$ technical replicates for KD2-250 cells, CTL-1000 cells, KD2-1000 cells, KD3-1000 cells; $n = 4$ for CTL-250 cells, KD1-250 cells, KD3-250 cells, KD1-1000 cells, unpaired t-test, two tail distribution. CTL vs. KD1, 250 cell: $P = 0.0064$, $t = 4.097$, d.f. = 6; CTL vs. KD2, 250 cell: $P = 0.062$, $t = 2.34$, d.f. = 5; CTL vs. KD3, 250 cell: $P = 0.001$, $t = 5.862$, d.f. = 6; CTL vs. KD1, 1,000 cell: $P = 0.0008$, $t = 7.135$, d.f. = 5; CTL vs. KD2, 1,000 cell: $P = 0.004$, $t = 5.82$, d.f. = 4; CTL vs. KD3, 1,000 cell: $P = 0.002$, $t = 7.163$, d.f. = 4. Error bars represent ± s.e.m. (**d**) EGFRvIII-*mOSMR*-KD1, -KD2, and - control astrocytes were cultured and cell number in each group was counted at 2, 4, and 6 d using a Nexcelom cell counter ($n = 9$ for control group day 4, $n = 6$ for all other groups, unpaired student t-test, two tail distribution. CTL vs. KD1, 2 d: $P = 0.004$, $t = 2.14$, d.f. = 14; CTL vs. KD2, 2 d: $P = 0.0008$, $t = 2.14$, d.f. = 14; CTL vs. KD1, 4 d: $P = 0.16$, $t = 2.14$, d.f. = 14, CTL vs. KD2, 4 d: $P = 0.09$, $t = 2.14$, d.f. = 14; CTL vs. KD2, 6 d: $P = 0.03$, $t = 2.13$, d.f. = 15; CTL vs. KD2, 6 d: $P = 0.09$, $t = 2.132$, d.f. = 15. Error bars represent ± s.e.m. (**e**) EGFRvIII-*mOSMR*-KD1, -KD2, and control astrocytes were subjected to staining with the antibody to the proliferation marker Ki67 and the DNA dye Hoechst. Graph represents quantification of percentage of astrocytes that were positive for Ki67 ($n = 3$ independent slides, CTL vs. KD1: $P = 0.05$, $t = 2.78$, d.f. = 4; CTL vs. KD2: $P = 0.047$, $t = 2.78$, d.f. = 4. Error bars represent ± s.e.m.

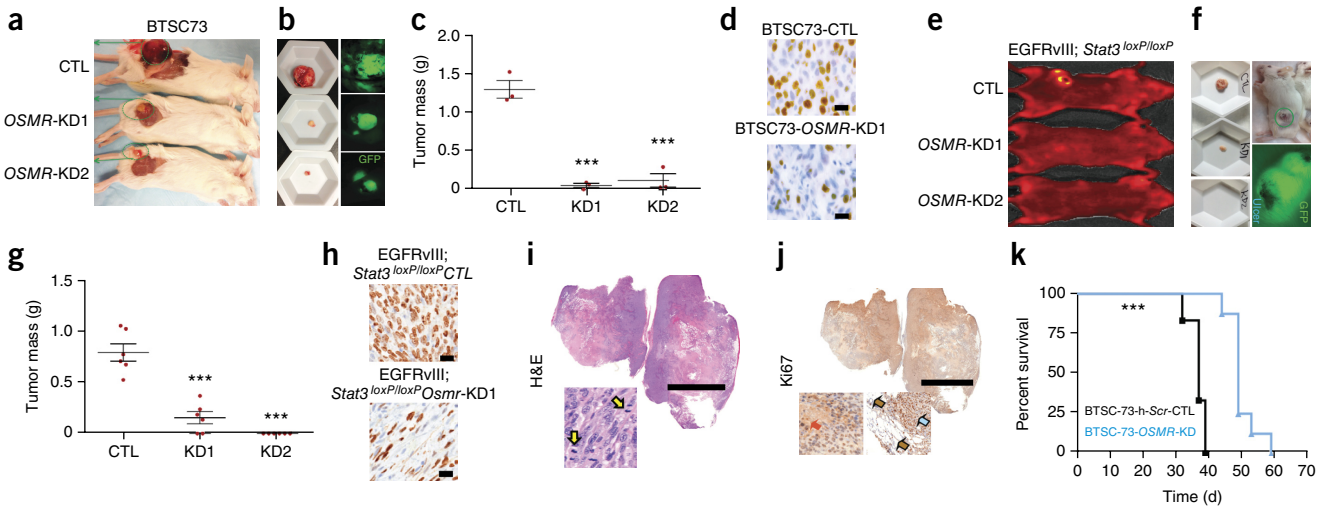

Figure 6 OSMR regulates the ability of EGFRvIII-expressing human BTSCs and mouse astrocytes to form tumors *in vivo*. (**a**) GFP-positive *OSMR*-KD1-, -KD2, or corresponding scramble control BTSC73 lines were injected into 6 week-old SCID mice and allowed to form tumors subcutaneously. Animals in each group were collected for tumor mass analyses as described in **c**. (**b**) Animals were photographed with a GFP filter to confirm presence of GFP positive tumors at the site of injection. (**c**) Tumors were weighed before fixation. Graph represents tumor mass for each group. $n = 3$ independent mice for each group. The significance of difference was analyzed using unpaired student *t*-test, two tail distribution. CTL vs. KD1: $P = 0.0004$, $t = 10.64$, d.f. = 4; CTL vs. KD2: $P = 0.0012$, $t = 8.22$, d.f. = 4. $^{***}P < 0.001$, Error bars represent ± s.e.m. (**d**) Immunohistochemical analyses of tumor sections obtained from mice injected with scramble control or *OSMR*-KD1-BTSC73 were performed using the Ki67 antibody. Scale bars, 20 µm. Image is representative of 6 independent section from three different mice. (**e**) *Osmr* knockdown and control EGFRvIII-expressing astrocytes, which also expressed GFP, were injected into 6 week-old SCID mice and allowed to form tumors subcutaneously. Animals were collected 4 weeks after injections at which time all mice injected with control EGFRvIII-expressing astrocytes were at end stage with ulcerated tumors. *Osmr*-KD1 and -KD2 and corresponding control were subjected to optical imaging to trace and detect tumors before their collection. (**f**) GFP-positive tumors were imaged using a fluorescence microscope (Top panel). (**g**) Isolated tumors were weighed before fixation. Graph represents quantification of the tumor mass in *Osmr* knockdown and control EGFRvIII-expressing astrocytes. The significance of difference was analyzed using unpaired student *t*-test, two tail distribution. $n = 6$ mice for each group. CTL vs. KD1: $P = 0.0001$, $t = 6.205$, d.f. = 10; CTL vs. KD2: $P = 0.0001$, $t = 9.338$, d.f. = 10. $^{***}P < 0.001$. Error bars represent ± s.e.m. (**h**) Ki67 staining of tumor section is presented for control and OSMR-KD1 astrocytes. No tumors were formed by *Osmr*-KD2 astrocytes. Image represents analyses of 6 different slides from three different mice. Scale bars, 20 µm. (**i**,**j**) EGFRvIII-STAT3$^{loxP/loxP}$ xenografts were subjected to immunohistochemistry using the Ki67 antibody or hematoxylin and eosin (H&E) staining to assess their characteristics. Scale bars, 5,000 µm; insets are at 80× magnification. Mitotic figures are shown with yellow arrows. Adipose tissue surrounding the tumor (brown arrows) is shown as negative control for Ki67 staining. Red arrow indicates necrotic area. Image represents slides from two independent mice. Blue arrow indicates tumor tissue. (**k**) Animals were injected with human BTSC73 cells and corresponding knockdown group as described in **a**. Each animal was collected at end stage. Kaplan-Meier survival plot was graphed to evaluate animal lifespan in each group. Black line, BTSC73-scrambled control, $n = 4$; Blue line: BTSC73-*OSMR*-knockdown, $n = 6$, $P = 0.0001$ by log rank test, $P = 0.0003$ by Gehan-Breslow-Wilcoxon test.

Expression of EGFRvIII typically occurs in glioblastoma tumors where EGFR is amplified[21–23]. We found that STAT3 also directly bound the promoter of *OSMR* in human BTSCs in which STAT3 is highly phosphorylated (**Fig. 2d** and **Supplementary Fig. 6c**), and analyses of the proteomic data at TCGA database revealed a positive correlation between the phosphorylation of EGFR/EGFRvIII at Tyr1068 with the phosphorylation of STAT3 at Tyr705 (**Supplementary Fig. 6d**). We therefore assessed the impact of OSMR knockdown on cell growth in BTSC145 cells that exhibit a high level of phosphorylated STAT3 using three *OSMR* knockdown lines (OSMR-KD1, OSMR-KD2 and OSMR-KD3). *OSMR* knockdown led to significant reduction in population growth of BTSC145 cells (**Fig. 5c**).

We next assessed whether OSMR regulates the proliferation of mouse astrocytes upon activation of EGFRvIII-STAT3 signaling. We used two short hairpin RNAs (shRNAs) targeting mouse *Osmr* mRNA that substantially reduced *Osmr* mRNA and OSMR protein levels in EGFRvIII-expressing astrocytes (**Supplementary Fig. 6e–g**). We found that the growth of EGFRvIII-expressing astrocytes was significantly reduced upon *Osmr* knockdown (**Fig. 5d**). Moreover, the percentage of Ki67-positive astrocytes was significantly reduced upon *Osmr* knockdown (**Fig. 5e** and **Supplementary Fig. 6h**).

OSMR is required for glioblastoma tumor growth

Our discovery of OSMR as a critical component of EGFRvIII-STAT3 signaling raised the question of whether OSMR regulates tumor growth *in vivo*. To determine the role of OSMR in tumorigenicity of human BTSCs *in vivo*, we subcutaneously injected two different *OSMR* knockdown or control BTSC73 lines, the latter infected with the scrambled shRNAs, into 6-week-old severe combined immunodeficient (SCID) mice and assessed the ability of these cells to form tumors *in vivo*. *OSMR* knockdown and control BTSC lines also expressed GFP, allowing confirmation that the tumors were initiated from the injected cells. Knockdown of *OSMR* in human BTSCs suppressed tumor growth by more than 80% (**Fig. 6a–c**). Immunohistochemical analyses using Ki67 antibody revealed that *OSMR* knockdown substantially attenuated cell proliferation in BTSC73-derived tumors *in vivo* (**Fig. 6d**).

To evaluate whether OSMR influences glial transformation *in vivo, OSMR* knockdown and control EGFRvIII-expressing astrocytes that also expressed GFP were injected subcutaneously into 6 week-old SCID mice. 2–3 weeks after injection, all mice in the control group harbored ulcerated tumors at the site of injection and had lost more than 20% of their body weight. We confirmed that the tumors initiated from the injected cells on the basis of GFP fluorescence (**Fig. 6e**,**f**).

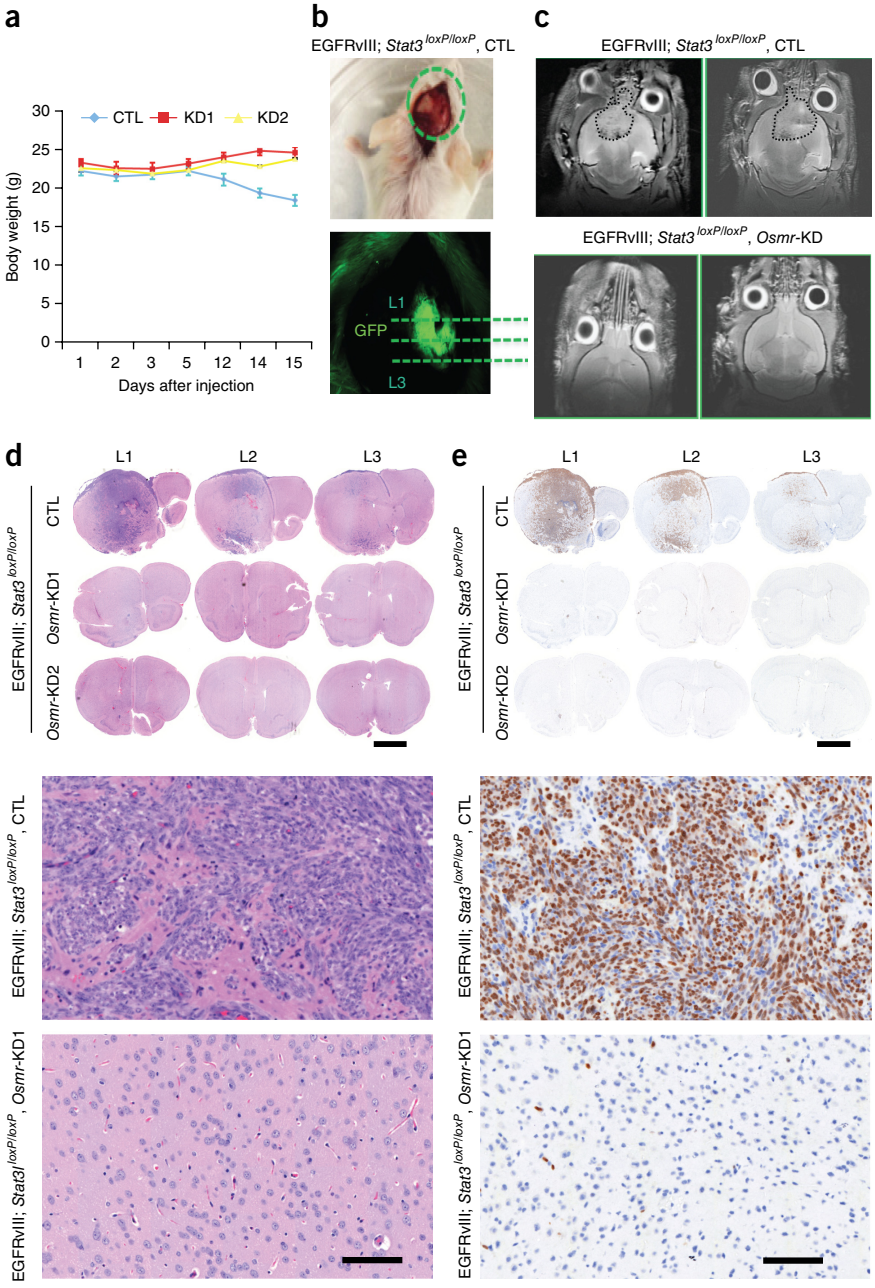

Figure 7 OSMR is required for brain tumor growth. (**a**) GFP-positive EGFRvIII-*Osmr*-knockdown or vector control EGFRvIII-expressing astrocytes were injected into SCID mice intracranially and allowed to form brain tumors. The graph represents quantification of animal weight from day 1 to day 15. CTL ($n = 5$); OSMR KD1 ($n = 3$), OSMR KD2 ($n = 3$). One mouse for OSMR-KD1 and one mouse for control were excluded from the analyses, as they did not survive the surgeries. All the surgeries were performed on the same day. CTL vs. KD1, day 15: $P = 0.0052$, $t = 5.25$, d.f. = 4; CTL vs. KD2, day 15: $P = 0.004$, $t = 5.022$, d.f. = 5; CTL vs. KD1, day 12: $P = 0.07$, $t = 2.4$, d.f. = 4; CTL vs. KD2, day 12: $P = 0.07$, $t = 2.26$, d.f. = 5. Error bars represent ± s.e.m. (**b**,**c**) Presence and absence of tumor was assessed by florescence imaging to detect GFP signal (**b**) and by MRI to detect tumor in each animal. Tumor periphery is shown with a dotted line (**c**). (**d**–**e**) Whole brains from the animals in each group were fixed in 10% formalin and subjected to immunohistochemical analyses by H&E and Ki67 staining. Three different sections (Level1 (L1), L2, and L3; each at 200 µm intervals) from each brain were analyzed. Presence of mitotic figures and highly proliferative cell population were detected in mice injected with control EGFRvIII-expressing astrocytes. None of the animals injected with either *Osmr*-KD1- or *Osmr*-KD2-EGFRvIII-expressing astrocytes exhibited these features. Representative magnification of stained sections in each group is shown in bottom panels. Each image is representative of 4 independent slides from two different mice for each group. Scale bars in upper panels, 1,000 µm; Scale bars in bottom panels, 100 µm.

We observed a dramatic reduction in tumor mass when EGFRvIII-expressing astrocytes were infected with an shRNA-expressing lentivirus to knock down *Osmr* (**Fig. 6e**–**g**). EGFRvIII-expressing, astrocyte-derived tumors were highly malignant with numerous mitotic bodies, necrosis and high Ki67 immunoreactivity (**Fig. 6i**,**j**). Similar to human BTSC73-derived tumors, immunohistochemical analyses of these tumors using Ki67 antibody showed that OSMR knockdown robustly attenuated cell proliferation *in vivo* (**Fig. 6h**). Quantification of tumor mass 4 weeks after injection showed that *OSMR* knockdown significantly suppressed tumor mass *in vivo* (**Fig. 6g**). The tumor-suppressive effect of OSMR knockdown correlated with the level of *OSMR* knockdown in the cells that had been injected (**Supplementary Fig. 6f**). Depletion of OSMR in human glioblastoma cells prolonged lifespan of animals injected with these cells (**Fig. 6k**). Taken together, these findings suggest that OSMR robustly influences the malignant transformation of EGFRvIII-expressing glial cells and human BTSC.

Having identified a critical role for OSMR in the malignant transformation and behavior of EGFRvIII-expressing mouse astrocytes and human BTSCs *in vivo*, we next asked whether OSMR contributes to tumorigenesis in the context of brain tissue *in vivo*. We injected intracranially EGFRvIII-expressing control and corresponding *OSMR* knockdown astrocytes into 6-week-old SCID mice. Mice injected with EGFRvIII-expressing control astrocytes formed brain tumors that were harvested when the animals were at end stage of disease and displayed a loss of body weight and neurological signs (**Fig. 7a** and data not shown). *OSMR* knockdown mice were collected at the same time for histological analyses. The tumors in the control animals were clearly derived from injected cells on the basis of GFP expression (**Fig. 7b**). Animals were also screened for the presence and absence of tumor by magnetic resonance imaging (MRI). In the imaging analyses, we detected tumors in all the animals injected with EGFRvIII-expressing astrocytes, but observed no tumors in animals injected with EGFRvIII-expressing *OSMR* knockdown astrocytes (**Fig. 7c**). Immunohistochemical analyses revealed the presence of highly malignant tumors in all brains injected with control EGFRvIII-expressing astrocytes (**Fig. 7d**–**e**). By contrast, no mitotic bodies, necrosis, hyper-proliferation or tumor mass were observed in the

animals injected with *OSMR* knockdown EGFRvIII-expressing astrocytes. These results establish that depletion of OSMR impedes brain tumor growth.

DISCUSSION

In this study, we discovered that the cytokine receptor OSMR is a required co-receptor of EGFRvIII that has a prominent role in glioblastoma tumorigenesis. We found that *OSMR* is a highly upregulated direct transcriptional target gene of STAT3 in glioblastoma. OSMR forms a complex with EGFRvIII to regulate STAT3 activation and its transcriptional output. Loss of OSMR impairs EGFRvIII function, STAT3 activation and brain tumor formation. Our study identified OSMR as a critical component of EGFRvIII-STAT3 signaling that forms a feed-forward signaling mechanism with these molecules to drive oncogenesis.

The transcription factor STAT3 exerts a dual role in glioblastoma tumors depending on the genetic background[17,24]. In the absence of the major oncogenic protein EGFRvIII, STAT3 has a tumor-suppressive role[17]. Further, STAT3 has an instructive role in astrocyte differentiation during neural precursor development[25]. However, expression of the oncogenic protein EGFRvIII triggers a switch, whereby STAT3 exerts a potent oncogenic function in glioblastoma[17,26,27]. We found that EGFRvIII-OSMR complex signals to activate STAT3, and STAT3 signals to upregulate OSMR expression. The result is a feed-forward signaling mechanism that drives oncogenesis. Accordingly, OSMR has a critical role in the mechanism that drives glioblastoma tumor progression.

In characterizing the underlying molecular mechanisms by which OSMR promotes EGFRvIII-STAT3 signaling, we found that the phosphorylation of EGFRvIII is required for binding to OSMR. Inhibition of EGFRvIII phosphorylation by lapatinib and carnatinib strongly impaired the EGFRvIII-OSMR interaction and STAT3 activation. Conversely, OSM has a critical role in EGFR phosphorylation, its interaction with OSMR and consequently STAT3 activation. We also observed that knockdown of OSMR attenuates EGFRvIII levels in EGFRvIII-expressing astrocytes. Together, our results suggest that EGFRvIII and OSMR are obligate co-receptors in maintaining oncogenic STAT3 signaling. Collectively, our findings suggest that OSMR and activated EGFR are components of a physical co-receptor complex that functionally cooperate to activate a common repertoire of target genes in glioblastoma tumors.

Wild-type EGFR has been reported to participate in the phosphorylation of EGFRvIII in glioma cell lines with EGFRvIII and EGFR overexpressed, though no direct interaction of EGFR and EGFRvIII has been reported in co-immunoprecipitation analyses of these cells[21,23]. In the present study, we did not detect an interaction between EGFR and EGFRvIII in human BTSCs or mouse astrocytes that expressed EGFRvIII. In light of these observations, it will be important in future studies to assess whether OSMR might facilitate the intimate relationship between wild-type EGFR and EGFRvIII in glioma cells with mixed composition.

Our findings reveal that the interaction of OSMR with wild-type EGFR is triggered by the ligand OSM in non-tumorigenic cells, suggesting that OSMR forms a co-receptor with wild-type EGFR in response to environmental cues. OSM is a multifunctional cytokine that is typically produced by white blood cells, but the production of OSM in cancer is thought to occur in the tumor stroma, suggesting the existence of cross-talk between the tumor stroma and cancer cells[28]. OSMR upregulation appears to confer increased sensitivity to OSM in cervical squamous carcinoma cells[29].

In conclusion, we identified a key mechanism that contributes to glioblastoma tumor progression. OSMR is a cell surface receptor that defines a feed-forward mechanism with EGFRvIII and STAT3 in glioblastoma pathogenesis, and thus represents an attractive target for the development of therapeutics. In particular, a screen for small molecules that either inhibit OSMR activity or its interaction with activated EGFR may prove valuable in identifying new drugs to mitigate the malignant behavior of glioblastoma tumors.

METHODS

Methods and any associated references are available in the online version of the paper.

Accession codes. Gene Expression Omnibus (GEO) accession codes for 12 RNA-seq and 2 ChIP-seq data sets are provided in **Supplementary Table 2** and are available under series GSE51281.

Note: Any Supplementary Information and Source Data files are available in the online version of the paper.

ACKNOWLEDGMENTS

These studies were carried out with support of grants to A.B. from the US National Institutes for Health (NS064007) and the Mathers Foundation, to M.A.R. from the US National Institutes for Health (R01AR044031), the Canadian Institutes for Health Research (CIHR, MOP-81288), and to A.J.-A. from the new investigator startup funds at the LDI/McGill University. M.A.R. is funded as the Canada Research Chair in Molecular Genetics. V.D.S. is funded as the Canada research chair in stem cell epigenetics. A.J.-A., H.Y. and N.C.C. were supported by postdoctoral fellowships from the CIHR. H.A.L. and S.W. are supported by grants from the Alberta Cancer Foundation and the Stem Cell Network. A.M.S. is supported by National Health and Medical Research Council grant and the Operational Infrastructure Support Program provided by the Victorian Government. We thank C. Porter at the Ottawa Hospital Research Institute for critical help with genomic data analyses.

AUTHOR CONTRIBUTIONS

A.J.-A., M.A.R., and A.B. designed the experiments, analyzed the data and wrote the manuscript. A.J.-A. performed the experiments and analyses. H.Y. and V.D.S. contributed to the analyses of RNA-seq and ChIP-seq data. T.H. contributed to RT-q-PCR, immunoblotting, immunostaining and tissue-culture work. H.A.L. contributed to the characterization of BTSCs and generation of STAT3-kncokdown BTSC73. N.C.C. contributed to PLA analyses and co-immunoprecipitation. M.-C.S. contributed to RT-q-PCR and ChIP-PCR. S.V.P. contributed to STAT3 microarray data in astrocytes. A.M.S. generated mouse EGFRvIII antibody. I.A.J.L. generated rabbit EGFRvIII-antibody. T.J.P. contributed to the bioinformatics analyses of TCGA and REMBRANDT data. K.L.L. generated and characterized BTSC 112, 139 and 145 cell lines. S.W. generated and characterized human BTSC12, 25, 30, 41, 68, 73, 90 cell lines.

COMPETING FINANCIAL INTERESTS

The authors declare no competing financial interests.

1. Stupp, R. *et al.* Radiotherapy plus concomitant and adjuvant temozolomide for glioblastoma. *N. Engl. J. Med.* **352**, 987–996 (2005).
2. Robins, H.I., Chang, S., Butowski, N. & Mehta, M. Therapeutic advances for glioblastoma multiforme: current status and future prospects. *Curr. Oncol. Rep.* **9**, 66–70 (2007).
3. Maher, E.A. *et al.* Malignant glioma: genetics and biology of a grave matter. *Genes Dev.* **15**, 1311–1333 (2001).
4. Furnari, F.B. *et al.* Malignant astrocytic glioma: genetics, biology, and paths to treatment. *Genes Dev.* **21**, 2683–2710 (2007).
5. Wen, P.Y. & Kesari, S. Malignant gliomas in adults. *N. Engl. J. Med.* **359**, 492–507 (2008).
6. Holland, E.C. Gliomagenesis: genetic alterations and mouse models. *Nat. Rev. Genet.* **2**, 120–129 (2001).
7. Bachoo, R.M. *et al.* Epidermal growth factor receptor and Ink4a/Arf: convergent mechanisms governing terminal differentiation and transformation along the neural stem cell to astrocyte axis. *Cancer Cell* **1**, 269–277 (2002).
8. Uhrbom, L. *et al.* Ink4a-Arf loss cooperates with KRas activation in astrocytes and neural progenitors to generate glioblastomas of various morphologies depending on activated Akt. *Cancer Res.* **62**, 5551–5558 (2002).
9. Bajenaru, M.L. *et al.* Optic nerve glioma in mice requires astrocyte Nf1 gene inactivation and Nf1 brain heterozygosity. *Cancer Res.* **63**, 8573–8577 (2003).

10. Louis, D.N. Molecular pathology of malignant gliomas. *Annu. Rev. Pathol.* **1**, 97–117 (2006).
11. Singh, S.K. *et al.* Identification of a cancer stem cell in human brain tumors. *Cancer Res.* **63**, 5821–5828 (2003).
12. Singh, S.K. *et al.* Identification of human brain tumour initiating cells. *Nature* **432**, 396–401 (2004).
13. Galli, R. *et al.* Isolation and characterization of tumorigenic, stem-like neural precursors from human glioblastoma. *Cancer Res.* **64**, 7011–7021 (2004).
14. Yuan, X. *et al.* Isolation of cancer stem cells from adult glioblastoma multiforme. *Oncogene* **23**, 9392–9400 (2004).
15. Wong, A.J. *et al.* Structural alterations of the epidermal growth factor receptor gene in human gliomas. *Proc. Natl. Acad. Sci. USA* **89**, 2965–2969 (1992).
16. Nagane, M., Lin, H., Cavenee, W.K. & Huang, H.J. Aberrant receptor signaling in human malignant gliomas: mechanisms and therapeutic implications. *Cancer Lett.* **162**, S17–S21 (2001).
17. de la Iglesia, N. *et al.* Identification of a PTEN-regulated STAT3 brain tumor suppressor pathway. *Genes Dev.* **22**, 449–462 (2008).
18. de la Iglesia, N., Puram, S.V. & Bonni, A. STAT3 regulation of glioblastoma pathogenesis. *Curr. Mol. Med.* **9**, 580–590 (2009).
19. Mosley, B. *et al.* Dual oncostatin M (OSM) receptors. Cloning and characterization of an alternative signaling subunit conferring OSM-specific receptor activation. *J. Biol. Chem.* **271**, 32635–32643 (1996).
20. Inda, M.M. *et al.* Tumor heterogeneity is an active process maintained by a mutant EGFR-induced cytokine circuit in glioblastoma. *Genes Dev.* **24**, 1731–1745 (2010).
21. Fan, Q.W. *et al.* EGFR phosphorylates tumor-derived EGFRvIII driving STAT3/5 and progression in glioblastoma. *Cancer Cell* **24**, 438–449 (2013).
22. Biernat, W., Huang, H., Yokoo, H., Kleihues, P. & Ohgaki, H. Predominant expression of mutant EGFR (EGFRvIII) is rare in primary glioblastomas. *Brain Pathol.* **14**, 131–136 (2004).
23. Zadeh, G., Bhat, K.P. & Aldape, K. EGFR and EGFRvIII in glioblastoma: partners in crime. *Cancer Cell* **24**, 403–404 (2013).
24. de la Iglesia, N. *et al.* Deregulation of a STAT3-interleukin 8 signaling pathway promotes human glioblastoma cell proliferation and invasiveness. *J. Neurosci.* **28**, 5870–5878 (2008).
25. Bonni, A. *et al.* Regulation of gliogenesis in the central nervous system by the JAK-STAT signaling pathway. *Science* **278**, 477–483 (1997).
26. Jahani-Asl, A. & Bonni, A. iNOS: a potential therapeutic target for malignant glioma. *Curr. Mol. Med.* **13**, 1241–1249 (2013).
27. Puram, S.V. *et al.* STAT3-iNOS Signaling Mediates EGFRvIII-Induced Glial Proliferation and Transformation. *J. Neurosci.* **32**, 7806–7818 (2012).
28. Caffarel, M.M. & Coleman, N. Oncostatin M receptor is a novel therapeutic target in cervical squamous cell carcinoma. *J. Pathol.* **232**, 386–390 (2014).
29. Winder, D.M. *et al.* Overexpression of the oncostatin M receptor in cervical squamous cell carcinoma cells is associated with a pro-angiogenic phenotype and increased cell motility and invasiveness. *J. Pathol.* **225**, 448–462 (2011).

ONLINE METHODS

Animals. Severe combined immunodeficient 6–8-week-old male mice were purchased from Charles River Laboratories. Mice with *Stat3* loxP-flanked (floxed) alleles (*Stat3*$^{loxP/loxP}$) were generated as described previously[30]. All animal experiments were conducted under the institutional guidelines and were approved by the Institutional Animal Care and Use Committee at the University of Ottawa and the Harvard University.

Cell culture. Primary human brain tumor cell lines (BTSC112, BTS139 and BTSC145) were initiated at the time of surgery after informed consent from adult glioblastoma patients according to BWH/Partners IRB protocol for use of excess/discarded tissue at the Harvard University. BTSC12, 25, 30, 41, 68, 73 and 90 cells were generated upon approval by the University of Calgary Ethics Review Board as described[31,32]. Cells derived from patient tumors were placed into culture directly after tumor isolation. Cells were maintained and grown in ultra-low-attachment flasks (Corning) in neurosphere (suspension) culture conditions. NeuroCult NS-A medium (Stemcell Technologies) supplemented with penicillin-streptomycin (1:100), heparin (2 µg/ml), human EGF (20 ng/ml) and human FGFb (10 ng/ml) was used to maintain all lines. BTSCs gave rise to non-adherent spheres following 1–3 weeks in culture. Primary tumor spheres were expanded and cryopreserved in 10% dimethyl sulfoxide (Sigma-Aldrich) until use in experiments. EGFRvIII status of BTSCs was determined by array CGH, CISH or as described[32].

OSMR knockdown BTSC73 lines were generated using lentiviruses carrying different *OSMR* shRNA plasmids. Three different shRNAs (Thermo Scientific, V3LHS_394103, V3LHS_394106 and #V2LHS_46203) were used to transduce BTSC73 line. *OSMR* knockdown BTSC73 lines were established by fluorescence-activated cell sorting (FACS) of the brightest GFP-positive live cells followed by antibiotic selection (1 µg/ml puromycin). Exposure of non-transduced BTSCs to 1 µg/ml of puromycin killed all cells within 3 d at this concentration (data not shown). *STAT3* knockdown BTSC73 line was generated by STAT3 shRNA constructs (Thermo Scientific, V3LHS_376018 and V2LHS_88502) as described[32]. As control, a lentivirus carrying a non-targeting construct (Thermo Scientific RHS4346) was used[32]. Generation of lentiviruses and cell transduction are described below.

Stat3 floxed (*Stat3*$^{loxP/loxP}$) astrocyte line was generated from mice with floxed *Stat3* alleles (*Stat3*$^{loxP/loxP}$) as described[17]. To generate *Stat3* knockout (*Stat3*$^{-/-}$), the genes flanked by *loxP* sites were excised *in vitro* using adenovirus encoding the recombinase Cre (University of Iowa). Primary astrocyte cultures were generated from postnatal day 2 B6 mice as described[33,34]. Murine stem cell virus (MSCV) control astrocytes and MSCV-EGFRvIII-expressing astrocytes were generated by retroviral mediated delivery of MSCV-EGFRvIII or MSCV plasmids into *Stat3*$^{loxP/loxP}$ astrocytes, and were immortalized by retroviral-mediated expression of the SV40 large T antigen protein as described[17]. *OSMR* knockdown EGFRvIII-expressing astrocytes were generated by lentivirus-mediated delivery of two different shRNA plasmids as described below. *OSMR* knockdown astrocytes were established by selection with blasticidin (5 µg/ml) in culture. Exposure of non-transduced astrocytes to 5 µg/ml completely killed the cells within 3 d in culture (data not shown).

Virus production and transduction. Recombinant lentiviruses were made by transfecting human embryonic kidney 293T (HEK293T) cells with lentiviral helper plasmids, pCMV-dR8.2 and pCMV-VS.VG (Addgene, 8455 and 8454), together with the transfer plasmid. Mouse *OSMR*-based lentiviruses were based on the pLKO.1 vector carrying the blasticidin resistance gene and obtained from the RNAi Consortium at the Broad Institute, as described[27]. Cloning of recombinant lentiviruses coding for shRNAs directed against mouse *Osmr* was performed by annealing and insertion of complementary oligonucleotides into stuffed-pLKO.1 plasmid using AgeI and EcoRI sites. Oligonucleotides were OSMRi1, forward: 5′-CCGG-ACGACTTTGACTTGGCGTAAA-CTCGAG-TTTACGCCAAGTCAAAGTCGTTTTTTG-3′; OSMRi1, reverse: 5′AATT CAAAAA-ACGACTTTGACTTGGCGTAAA-CTCGAG-TTTACGCCAA GTCAAAGTCGT-3′; OSMRi2, forward: 5′-CCGG-TTGGAACTGGACGT CTGATAT-CTCGAG-ATATCAGACGTCCAGTTCCAA-TTTTTG-3′; OSMRi2, reverse: 5′-AATTCAAAAA-TTGGAACTGGACGTCTGATAT-CTCGAG-AT ATCAGACGTCCAGTTCCAA-3′.

Correct insertion of the desired oligonucleotides was confirmed by sequencing. As control, pLKO.1–TRC026 containing the null-T sequence[27] or pLKO.1- scramble (Addgene, 26701)[35] were used. Viral supernatants were collected and purified using Speedy Lentivirus Purification kit (ABM, LV999-1) according to the manufacturer's recommendation. Purified lentiviruses were used immediately without exposure to any freeze-thaw cycles. BTSC73 was transduced with lentiviral particles at the time of plating. Briefly, purified lentiviruses were diluted in 500 µl of BTSC medium in a 1.5 ml Eppendorf tube. In parallel, 1 million cells were resuspended in 500 µl of BTSC medium in a 1.5-ml eppendorf tube. The media containing cells and viruses were combined, mixed and plated into 6-well ultra-low-attachment surface plates (Costar, 3471). 2 ml of additional medium was added to each well following 6–8 h. Following 1 week in culture, brightest GFP positive transgenic BTSCs were selected by FACS and maintained in 1 µg/ml of puromycin. EGFRvIII-expressing astrocytes were infected in 3-cm dishes by incubating for 24 h with the corresponding lentivirus, following which the medium was switched. Cells were expanded into 10-cm plates and selected with blasticidin at a concentration of 5 µg/ml. *OSMR* knockdown astrocytes and corresponding controls were expanded and frozen into cell stocks for use in biochemical and functional assays.

Whole-transcriptome analyses (RNA-seq). Total RNA was isolated from BTSC lines or astrocytes by the RNeasy kit (Qiagen). The quality of RNA was assessed by bioanalyzer before sequencing. Libraries for poly(A)$^+$ RNA were prepared according to the Illumina protocol. Libraries were sequenced on Illumina GAIIX Genome Analyzer or on HI-SEQ 2000 platforms. RNA-seq reads were mapped and analyzed by TopHat/Cufflinks RNA-seq analysis pipeline using default parameters. Differentially expressed genes were called by CuffDiff using default parameters. Gene ontology of expression data was done using the functional annotation module of DAVID 6.7 (http://david.abcc.ncifcrf.gov)[36].

RT-q-PCR analyses. RNA was prepared from cells using Trizol extraction and purification. cDNA was prepared using oligo(dT) primers and SuperScript III First-Strand cDNA synthesis system (Invitrogen) according to the protocol of the manufacturer. Quantitative PCR was performed using the SYBR Green 1 Master Kit on a Lightcycler Mx3000p (Stratagene).

Chromatin immunoprecipitation. Cells were washed with PBS containing protease inhibitors (Aprotinin, 1 µg/ml; Leupeptin, 5 µg/ml, Pepstatin A, 1 µg/ml; and PMSF, 1 mM) before fixation. Cells were cross-linked with 1% formaldehyde in PBS for 10 min, and quenched with a solution containing 0.125 M glycine in PBS for 5 min at room temperature. For nonadherent BTSCs, washing, fixing and quenching of the cells were performed in 15-ml Falcon tubes with cells rotating at room temperature. For adherent astrocytes, cells were washed, fixed and quenched in 15-cm plates. Following quenching, cells were washed with PBS containing protease inhibitors twice, and cell pellets were collected by spinning at 1,000 r.p.m. for 10 min at 4 °C. Pellets were dissolved in ChIP lysis buffer (40 mM Tris-HCl, pH 8.0, 1.0% Triton X-100, 4 mM EDTA and 300 mM NaCl) containing protease inhibitors. Chromatin was fragmented by sonication in a water bath Bioruptor at 4 °C to an average length of 500 base pairs (bp) for ChIP-qPCR analyses and to an average length of 150 bp for ChIP-seq analyses. The lysates were spun at 14,000 r.p.m. for 15 min, and the supernatant was diluted 1:1 in ChIP dilution buffer containing 40 mM Tris-HCl, pH 8.0, and 4 mM EDTA plus protease inhibitors. Immunoprecipitation was done using a ChIP-grade STAT3 antibody (Cell Signaling Technology, 9132) against the endogenous STAT3 protein or with a rabbit IgG (Millipore, 12-370) in control ChIP. Antibody–protein–DNA complexes were collected, washed and eluted, and the cross-links were reversed as described previously[37–39]. Immunoprecipitated DNA was analyzed by q-PCR and binding enrichment was expressed as % input. For ChIP-Seq experiments, 10 ng of immunoprecipitated DNA from both the experiment and control ChIP were submitted for sequencing.

ChIP-PCR sequences (h: human, m: mouse) were h*STAT3* Fw: GTGC TGGCTGTTCCGACAGTT; h*STAT3* Rv: AGAGGGAGCTGTATCAGGG GCATT; h*OSMR* Fw: GACTGAAGGGAGGGAATTCCTGT; h*OSMR* Rv: CAATTTCCCGTCTTGCTG; h*HPRT* Fw: CGGTAGGTTTGGGAATCA; h*HPRT* Rv: CAGTTTGCAGGCTCACTA; h*HBB* Fw: CTGTTTGAGGTTGCTAGTG; h*HBB* Rv: TCATCACTTAGACCTCACC; m*Stat3* Fw: TCTGAGAGCTTT GTGCTCCT; m*Stat3* Rv: GAGCCGTATCAGGGCATTTA; m*Osmr* Fw: AATCAACTACGGGGCAAGTG; m*Osmr* Rv: ACCAGGAGCAAATTCCTGTG; m*Chr5* Fw: TGTGGCTATGCTGGTTCAAG; m*Chr5* Rv: GGGGAATGAGT TTTGGTGTG.

doi:10.1038/nn.4295

ChIP-seq peak calling and analyses. The ChIP DNA library was prepared according to the Illumina protocol. Sequencing reads (36 bp) were generated on Illumina GAIIX Genome Analyzer or on HI-SEQ 2000 platforms. Sequenced reads with identical 5′ ends were counted as one to avoid PCR-induced sequencing bias. Sequences were mapped to the mouse genome assembly (mm9) using the Illumina GA analysis pipeline ELAND with standard parameters, allowing up to two mismatches. The ELAND output of ChIP-seq data are available in GEO as the series and control samples. 7,725 regions with enriched STAT3 ChIP-seq reads (STAT3 peaks) were identified by BayesPeak with posterior probability equal or more than 0.995. 16,078 negative peaks were called by BayesPeak with flipped STAT3 ChIP-seq data set and IgG ChIP-seq data set and represent genomic regions enriched by IgG comparing to the STAT3 antibody. Of those, 7,672 negative peaks with identical length distribution as STAT3 ChIP-seq peaks were randomly selected from the total negative peak pool and included in this study as negative control. As additional controls, random peak set were established and defined as randomly selected genomic regions with identical length distribution as STAT3 peaks. Peaks were annotated with their location relative to transcription start sites (Ensemble). Peaks greater than 800 bp were excluded from further analysis, based on the size of excised ChIP fragments used for Solexa sequencing. Peak height was calculated as number of tags per 100 bp. Peaks were sorted in order of decreasing peak height for further analyses. Conservation scores of STAT3 and negative control peaks were determined using the UCSC placental mammal conservation track.

ChIP-seq motif analyses. For peak motif analysis, we used the motif-based sequence analyses tool Multiple EM for Motif Elicitation (MEME)[40] to search for motifs in the 50 bp around the summit of the top 1,000 STAT3 peaks (ranked by BayesPeak score). Peak sequences using these motifs were input into weblogo to generate a representation of the motifs found in each peak subset. The position weight matrix (PWM) of each motif was passed to Find Individual Motif occurrences (FIMO) tool[41] to identify motif instances in 200-bp sequences around the summit of all STAT3 peaks and negative peaks.

Analyses of TCGA and REMBRANDT public databases. Kaplan-Meier survival plots were generated using REMBRANDT and TCGA databases.

To generate TCGA Kaplan-Meier survival plots, we downloaded the raw data from TCGA (https://genome-cancer.ucsc.edu). We searched for data sets involving glioblastoma multiforme (GBM), selecting a HiSeq gene expression data set with 172 total samples. Using the visual data browser, we selected 'gene' mode and typed in the gene of interest to access their expression values. We 'copied' these values to the 'clinical variables' side of the browser, by creating 'signatures' for each one. We also added a number of clinical variables to the default list, including 'overall survival indicator' and 'overall survival'. The first of these has one of two values for most samples: 1 = the patient died, 0 = the patient was last known to be alive. The second value records the number of days after initial diagnosis at which the patient died (in case of death) or was last followed up (in case of alive). We then downloaded the data (using TCGA download tool) as a tab-separated text file. We imported that file into Matlab (programming and data analysis platform) for further work. We removed from the analysis any patients not explicitly listed as dead or alive (there were 8 patients). This left 113 dead patients and 52 alive patients. For each of the genes of interest (*OSMR* or *STAT3*), we divided the patients into two classes (high and low) based on their expression for the gene being ≥ median or < median, respectively. We performed a Kaplan-Meier survival analysis using a standard custom script as described in Bewick *et al.*, 2004 (ref. 42). For this analysis, as is standard, the alive patients were considered as 'censored' data. Significance of difference between the two groups was computed by the chi-squared statistic comparing total expected death events for each group (under null hypothesis of same death rates at every time) to observed death events.

To generate REMBRANDT Kaplan-Meier survival plots, the survival data were not available for download using online tools at REMBRANDT. We therefore downloaded a 300 MB compressed archive of all the data related to the project, providing us access to the raw survival data for glioblastoma-only patients in the REMBRANDT database. The data are now available at https://gdoc.georgetown.edu/gdoc/ or can be obtained by contacting REMBRANDT. The raw data were subjected to similar analyses as described for TCGA data above.

Immunoblotting, immunostaining and antibodies. Total protein was harvested in RIPA lysis buffer containing protease inhibitors (Complete-Mini; Roche-Boehringer). Protein concentration was determined by Brad.f.ord assay (Bio-Rad), after which samples (5–25 µg each) were subjected to SDS-PAGE and electroblotted onto Immobilon-P membrane (Millipore). Membranes were blocked in 5% nonfat milk or 5% bovine serum albumin (BSA) in PBST, before sequential probing with primary antibody and HRP-conjugated secondary antibody in blocking solution. Target proteins were visualized by ECL (Amersham-Pharmacia) with Biomax XAR film (Kodak). Primary antibodies used were: anti-Phospho-STAT3 (1:1,000; Cell Signaling, 9138 and 9134); anti-STAT3 (1:1,000, Cell Signaling, 9132); anti-OSMR (1:500, Abnova, H00009180-B01p; 1:250, Santa Cruz, 8494; 1:500 Abcam, 85575), p-EGFR (1:1,000, Abcam 5644; 1:500, Cell Signaling, 2234), and EGFR (1:500, Cell Signaling, 2232). The full scans of western blots in the main figures and supplemental figures are presented in **Supplementary Figures 7** and **8**, respectively.

For immunostaining, cells were fixed in 4% paraformaldehyde (PFA) for 20 min and subsequently permeabilized with 0.04% TritonX in PBS. Tumor tissues were fixed in 10% formalin, embedded in Paraplast, and serially sectioned at 5 µm. Sections were deparaffinized through xylenes and graded ethanol, and subsequently stained with hematoxylin and eosin for histological evaluation. Proliferating cells were stained with a rabbit polyclonal antibody to Ki67 (Vector Laboratories), and the immunolabeling was visualized with the Vectastain Elite ABC Reagent and DAB Substrate Kit (Vector Laboratories). Sections were counterstained with hematoxylin.

Proximity ligation assay. PLAs were performed using the Duolink II Detection Reagents Red (Olink) according to the manufacturer's protocol. PLA signals were detected by confocal microscopy (Zeiss, LSM 510 meta). Quantification of PLA signals was performed blind to the different groups.

Protein immunoprecipitation. Immunoprecipitation (IP) was performed from whole-cell extracts of astrocytes or BTSCs as indicated. Cells were lysed for 30 min on ice in lysis buffer (50 mM Tris pH 7.5, 150 mM NaCl, 2 mM $MgCl_2$, 0.5 mM EDTA, 0.5% Triton X-100, protease inhibitor cocktail). Lysates were cleared by centrifugation (14.8K) for 20 min at 4 °C, and subsequently incubated with either anti-OSMR antibody (Abnova) or EGFRvIII antibody (this antibody is described in ref. 43.) or mouse IgG (Millipore) as a control. As an additional control, lysis buffer without cell lysate was incubated with anti-OSMR antibody. Primary antibody incubations were carried out overnight at 4 °C, followed by a 1-h incubation at 4 °C with Protein A-agarose (Sigma-Aldrich). Beads were washed three times with lysis buffer and eluted by boiling in SDS sample buffer. Immunoprecipitates were analyzed by immunoblotting using the antibodies indicated.

Proliferation and survival assays. All cell-counting experiments were performed in a blinded fashion to the different groups. For cell-counting experiments, astrocytes or BTSCs were plated at a density of 20,000 cells per 6-cm plate. For astrocytes, cells were washed with 1× PBS, trypsinized, and counted 2–6 d after plating using a cellometer auto T4 (Nexcelom Bioscience). For all experiments, cells were also lysed 2 h after plating to ensure that equal numbers were initially plated across conditions. For BTSCs, media containing floating cells were collected. Cells were harvested and dissolved in BTSC medium. Cells were counted 4–8 d after plating using a Cellometer Auto T4. For Alamar blue assay, 100–1,000 cells were dissolved in 180 µl of medium and added to each well of a 96-well plates and incubated at 37 °C. 20 µl of 10× PrestoBlue cell viability reagent (Invitrogen, A13261) was added to each well 5–10 d following plating. Cultures were incubated for 4–14 h (depending on cell number plated) with PrestoBlue cell viability reagents, following which the wells were read using a fluorescence plate reader (excitation wavelength 530/25, emission wavelength, 590/35). Wells containing medium only were used to determine background signal. For each condition, cells were plated in triplicate. For Ki67 staining, cells were fixed and stained with Ki67 and Hoechst as described above. Percentage of Ki67 positive cells in each field was obtained by dividing total number of Ki67 positive cells over total number of cells. Three random fields were counted across each slide.

Mouse injections and tumor assays. BTSC or astrocyte cultures were dissociated into single-cell suspensions in serum-free, antibiotic-free medium. One million (astrocytes) to five million (BTSC73) cells were injected

subcutaneously into 6-week-old male SCID mice. Mice were killed, and the tumors were removed, measured and fixed for histological analyses at the time they developed neurological signs and ulcerated tumors. For Kaplan-Meier survival plots, mice were collected at the time they were at end stage. Median survivals were determined by a log-rank test using GraphPad Prism as described previously[32]. For intracranial injections, 3×10^5 EGFRvIII-expressing OSMR-KD1, -KD2 and corresponding control were redissolved in serum-free medium and were stereotactically implanted into the right striata of 6-week-old male SCID mice. Animals were killed after 4 weeks of injections. Brains were removed, fixed in 10% formalin, and prepared for histology and immunohistochemistry analyses. MRI and cranial dissection were performed to confirm presence of tumor.

Statistical analyses. Analyses for high-throughput sequencing data are described above. Statistical analyses for TCGA and REMBRANDT database are described above. Statistical analyses for functional and biochemical *in vitro* and *in vivo* studies were performed using two-tailed distribution unpaired Student *t*-test. All dot plots were generated by Graphpad Prism 6. All histograms were presented as mean ± s.e.m. *P* values of equal or less than 0.05 were considered significant and are marked with an asterisk on the histogram. *P* values of less than 0.01 are denoted by **, and *P* values of less than 0.001 are denoted by *** on the histograms. Median survival data were determined by a log-rank test using GraphPad Prism as described previously[32]. No statistical methods were used to predetermine sample sizes, but our sample sizes are similar to those generally used in the field. Data distribution was assumed to be normal, but this was not formally tested. Blinding and randomization was performed on all counting experiments including cell number quantification, Ki67 staining, and PLA signal quantification, and survival data analyses.

A **Supplementary Methods Checklist** is available.

30. Raz, R., Lee, C.K., Cannizzaro, L.A., d'Eustachio, P. & Levy, D.E. Essential role of STAT3 for embryonic stem cell pluripotency. *Proc. Natl. Acad. Sci. USA* **96**, 2846–2851 (1999).
31. Kelly, J.J. *et al.* Proliferation of human glioblastoma stem cells occurs independently of exogenous mitogens. *Stem Cells* **27**, 1722–1733 (2009).
32. Luchman, H.A. *et al.* An in vivo patient-derived model of endogenous IDH1-mutant glioma. *Neuro. Oncol.* **14**, 184–191 (2012).
33. Di Giorgio, F.P., Carrasco, M.A., Siao, M.C., Maniatis, T. & Eggan, K. Non-cell autonomous effect of glia on motor neurons in an embryonic stem cell-based ALS model. *Nat. Neurosci.* **10**, 608–614 (2007).
34. Nagai, M. *et al.* Astrocytes expressing ALS-linked mutated SOD1 release factors selectively toxic to motor neurons. *Nat. Neurosci.* **10**, 615–622 (2007).
35. Bryant, D.M. *et al.* A molecular network for *de novo* generation of the apical surface and lumen. *Nat. Cell Biol.* **12**, 1035–1045 (2010).
36. Huang, W., Sherman, B.T. & Lempicki, R.A. Bioinformatics enrichment tools: paths toward the comprehensive functional analysis of large gene lists. *Nucleic Acids Res.* **37**, 1–13 (2009).
37. Soleimani, V.D., Palidwor, G.A., Ramachandran, P., Perkins, T.J. & Rudnicki, M.A. Chromatin tandem affinity purification sequencing. *Nat. Protoc.* **8**, 1525–1534 (2013).
38. Soleimani, V.D. *et al.* Transcriptional dominance of Pax7 in adult myogenesis is due to high-affinity recognition of homeodomain motifs. *Dev. Cell* **22**, 1208–1220 (2012).
39. Soleimani, V.D. *et al.* Snail regulates MyoD binding-site occupancy to direct enhancer switching and differentiation-specific transcription in myogenesis. *Mol. Cell* **47**, 457–468 (2012).
40. Bailey, T.L., Williams, N., Misleh, C. & Li, W.W. MEME: discovering and analyzing DNA and protein sequence motifs. *Nucleic Acids Res.* **34**, W369–W373 (2006).
41. Grant, C.E., Bailey, T.L. & Noble, W.S. FIMO: scanning for occurrences of a given motif. *Bioinformatics* **27**, 1017–1018 (2011).
42. Bewick, V., Cheek, L. & Ball, J. Statistics review 12: survival analysis. *Crit. Care* **8**, 389–394 (2004).
43. Lavictoire, S.J., Parolin, D.A., Klimowicz, A.C., Kelly, J.F. & Lorimer, I.A. Interaction of Hsp90 with the nascent form of the mutant epidermal growth factor receptor EGFRvIII. *J. Biol. Chem.* **278**, 5292–5299 (2003).

doi:10.1038/nn.4295